

## BIFURCATION OF THE HODGKIN AND HUXLEY EQUATIONS: A NEW TWIST

■ J. GUCKENHEIMER  
Mathematics Department,  
Cornell University,  
Ithaca, NY 14853, U.S.A.

■ I. S. LABOURIAU  
Departamento de Mathematica Aplicada,  
Universidade do Porto,  
4000 Porto, Portugal

(E.mail: GUCKEN@MACOMB.TN.CORNELL.EDU)

The Hodgkin and Huxley equations model action potentials in squid giant axons. Variants of these equations are used in most models for electrical activity of excitable membranes. Computational tools based upon the theory of nonlinear dynamical systems are used here to illustrate how the dynamical behavior of the Hodgkin Huxley model changes as functions of two of the system parameters.

**1. Introduction** A nerve cell's response to constant electrical stimulation varies according to the cell's characteristics as well as the experimental setting. Two common types of responses are single voltage pulses (action potentials) and trains of impulses of various lengths (Jack *et al.*, 1975). The space-clamped Hodgkin and Huxley equations for the nerve impulse (denoted HH throughout this paper) are a system of four nonlinear ordinary differential equations that relate the difference of electric potential across the cell membrane of a squid giant axon to the membrane's permeability to  $\text{Na}^+$  and  $\text{K}^+$  ions as a response to an externally applied current stimulus. The equations contain several auxiliary parameters (Hodgkin and Huxley, 1952b) representing equilibrium potentials of ions, maximum conductance of ion channels and temperature. The work of Hodgkin and Huxley was a landmark of biophysics and their equations are a prototype for most quantitative models for the electrophysiological properties of membranes that have been studied subsequently. Despite the importance of HH, understanding of the qualitative properties of their solutions is fragmentary (Hille, 1992).

We study systematically how an axon changes its type of response from repetitive firing to single action potentials, in the context of the HH equations. Our approach relies upon the use of multiparameter bifurcation theory, a part of the modern theory of nonlinear dynamical systems. In particular, we

describe how periodic and equilibrium solutions change as functions of the parameters representing the stimulus intensity  $I$  and the potassium reversal potential  $\bar{V}_K$ . By assuming that this two-parameter system is *generic* we describe the codimension one and two bifurcations that appear to divide the parameter plane into regions with different structurally stable phase portraits. The work described here is probably of more interest for the computational tools that it introduces than for the particular results about the HH equations. It establishes a methodology for obtaining much more extensive dynamical information from models of electrically excitable membranes than has been available heretofore. Our results point towards inherent limitations in the possibilities for qualitatively capturing the complete repertoire of dynamical behavior displayed by the HH equations in a planar vector field.

The HH equations are given in Section 2 and their bifurcations are described in Section 4. We present bifurcation diagrams for HH on the  $I \times \bar{V}_K$  plane that are conjectured on the basis of symbolic calculations, numerical computations and visual examination of a large number of phase portraits. The singular points of these bifurcation diagrams are characterized in terms of codimension one and two bifurcations of vector fields in the plane, which are described in Section 3. We examine two values of the potassium permeability  $\bar{g}_K$  and use this information to illustrate the sensitivity of the HH equations to changes in other parameters. Between the two chosen values of  $\bar{g}_K$  there is a codimension three bifurcation whose unfolding has been determined (Guckenheimer, 1986). The changes between the bifurcation diagrams are consistent with this analysis. Our results are discussed briefly in Section 5.

**2. The Space Clamped HH Equations.** The HH equations (Hodgkin and Huxley, 1952) relate the difference in electric potential across the cell membrane ( $V$ ) and gating variables ( $m$ ,  $n$  and  $h$ ) for ion channels to the stimulus intensity ( $I$ ) and temperature ( $T$ ), as follows:

$$\left\{ \begin{array}{l} \dot{V} = -G(V, m, n, h) + I \\ \dot{m} = \Phi(T)[(1-m)\alpha_m(V) - m\beta_m(V)] \\ \dot{n} = \Phi(T)[(1-n)\alpha_n(V) - n\beta_n(V)] \\ \dot{h} = \Phi(T)[(1-h)\alpha_h(V) - h\beta_h(V)], \end{array} \right.$$

where  $\dot{x}$  stands for  $dx/dt$  and  $\Phi$  is given by  $\Phi(T) = 3^{(T-6.3)/10}$ . The other functions involved are:

$$G(V, m, n, h) = \bar{g}_{Na} m^3 h (V - \bar{V}_{Na}) + \bar{g}_K n^4 (V - \bar{V}_K) + \bar{g}_L (V - \bar{V}_L)$$

and the equations modeling the variation of membrane permeability are:

$$\begin{aligned}\alpha_m(V) &= \Psi\left(\frac{V+25}{10}\right) & \beta_m(V) &= 4e^{V/18} \\ \alpha_n(V) &= 0.1\Psi\left(\frac{V+10}{10}\right) & \beta_n(V) &= 0.125e^{V/80} \\ \alpha_h(V) &= 0.07e^{V/20} & \beta_h(V) &= (1 + e^{(V+30)/10})^{-1}\end{aligned}$$

with

$$\Psi(x) = \begin{cases} x/(e^x - 1) & \text{if } x \neq 0 \\ 1 & \text{if } x = 0. \end{cases}$$

Notice that  $\alpha_y(V) + \beta_y(V) \neq 0$  for all  $V$  and for  $y = m, n$  or  $h$ . The parameters  $\bar{g}_{\text{ion}}$  and  $\bar{V}_{\text{ion}}$  representing maximum conductance and equilibrium potential for the ion were obtained from experimental data by Hodgkin and Huxley, with the values given below:

$$\begin{aligned}\bar{g}_{\text{Na}} &= 120 \text{ mS/cm}^2, & \bar{g}_{\text{K}} &= 36 \text{ mS/cm}^2, & \bar{g}_{\text{L}} &= 0.3 \text{ mS/cm}^2, \\ \bar{V}_{\text{Na}} &= -115 \text{ mV}, & \bar{V}_{\text{K}} &= 12 \text{ mV}, & \bar{V}_{\text{L}} &= 10.599 \text{ mV}.\end{aligned}$$

The values of  $\bar{V}_{\text{Na}}$  and  $\bar{V}_{\text{K}}$  can be controlled experimentally (Hodgkin and Huxley, 1952a; Jack *et al.*, 1975). For all the results in this paper we use the temperature  $T=6.3^\circ\text{C}$  and, except where stated explicitly, all the other parameters involved in HH have the values quoted above that we call *HH values*.

The HH equations define a four-dimensional vector field that determines how values of  $(v, m, n, h)$  evolve in time. For fixed parameter values the four-dimensional space representing values of  $(v, m, n, h)$  will be filled with curves, called **trajectories** that are the solutions to the HH equations. The geometry of how the trajectories partition the four-dimensional space constitutes the **phase portrait** of the dynamical system. Prominent features of the phase portraits are special trajectories: **equilibrium points** at values of  $(v, m, n, h)$  at which the HH equations vanish and **periodic orbits** consisting of trajectories that return to their initial point some later time (Guckenheimer and Holmes, 1983). The **stable manifold** of an equilibrium or periodic orbit is the set of trajectories that approach it in forward time. Similarly, the **unstable manifold** of an equilibrium or periodic orbit is the set of trajectories that approach it in backwards time.

**3. A Bifurcation Dictionary.** As parameters of a dynamical system are varied qualitative changes in the phase portrait may occur at special values of the parameters. These changes are called **bifurcations**. In generic families of vector

fields only limited patterns of bifurcation occur (Guckenheimer and Holmes, 1983). Bifurcations in generic two-parameter families of systems have been studied extensively. They form **organizing centers** (Thom, 1975), whose structure can be used as the key ingredient in guiding computation of the bifurcation diagrams for specific examples. The bifurcations that occur in our study of HH are listed below. In each case we consider a parametrized family of ordinary differential equations,  $\dot{x} = f(x, \mu)$ , with  $x \in \mathbf{R}^n$  and  $\mu \in \mathbf{R}^2$ , undergoing bifurcation at  $\mu = \mu_0$  and we describe its behavior for values of the parameter  $\mu$  near  $\mu_0$ . The **codimension** of a bifurcation is the minimum dimension of a parameter space in which the bifurcation may occur in a persistent way. For each bifurcation of codimension two there is a “map” of parameter space, called a **bifurcation diagram**, showing the different local qualitative phase portraits of the differential equation that correspond to each subset of parameter values. Detailed descriptions and analysis of the different types of bifurcations can be found in the current literature, for instance Dangelmayr and Guckenheimer (1987), Guckenheimer (1986) and Guckenheimer and Holmes (1983).

*Codimension 1 bifurcations.*

**Saddle node or fold (sn).** Two equilibrium points coalesce and disappear.

**Hopf bifurcation (h).** The amplitude of a periodic orbit decreases until it is reduced to a point and disappears while its period approaches a positive limit as  $\mu \rightarrow \mu_0$ .

**Saddle loop or homoclinic bifurcation (sl).** The amplitude of a periodic orbit may increase until it captures a saddle point and disappears, its period tending to infinity as  $\mu \rightarrow \mu_0$ .

**Twisted saddle loops (tsl)** (Chow *et al.*, 1988). An orientation reversal along a homoclinic orbit may occur in systems whose dimension is larger than two. A generic homoclinic orbit is in a two-dimensional ribbon which is invariant under the flow with tangents in the directions of the weakest contraction and expansion at the saddle point. A twisted saddle loop occurs if this ribbon is not orientable.

**Double cycle or saddle node of cycles (dc).** Two periodic orbits coalesce and disappear.

**Period doubling (pd).** At a period doubling bifurcation a periodic orbit changes its stability, while a periodic orbit of twice its period coalesces with the bifurcating periodic orbit.

*Codimension 2 bifurcations.*

**Cusp (c).** Three equilibrium points coalesce into one.

**Takens–Bogdanov bifurcation (tb).** The linearization of  $F(x, \mu_0)$  at the

equilibrium point has a double zero eigenvalue. Adjacent to the *tb* bifurcation are curves of saddle node, saddle loop and Hopf bifurcations. The cycle involved in the Hopf bifurcation is destroyed at a saddle loop.

**Neutral saddle loop (nsl).** The stability of the periodic orbit involved in a saddle loop bifurcation is determined by the sum of two eigenvalues of the saddle. In a two-parameter family of vector fields this stability may change at a point where the sum of eigenvalues is zero (Guckenheimer, 1986). A curve of double cycles terminates at this point.

**Twisted neutral saddle loop (tsl).** When a neutral saddle loop occurs along a twisted homoclinic orbit its unfolding is substantially different than in the orientation preserving case (nsl) that occurs in the plane. There are adjacent curves of orientation and twisted saddle loop bifurcations, as well as a curve of period doubling bifurcations (Chow *et al.*, 1988; Kokubu, 1988; Yanagida, 1987).

**Saddle node loop (snl).** At a saddle node there is a homoclinic orbit (Schecter, 1987). Adjacent to a saddle node loop are curves of the saddle nodes and saddle loops.

**Degenerate Hopf bifurcation (dh).** There is a degeneracy in the way in which periodic orbits collapse onto an equilibrium point at a Hopf bifurcation (dh) (Takens, 1974).

**4. HH Bifurcations.** This section describes the bifurcations of the HH equations and the techniques that were used to find them. The bifurcations are divided into two categories: local and global. Local bifurcations are those that can be calculated in terms of the derivatives of the HH equations at the equilibrium points. Global bifurcations can be studied only by numerically integrating the HH equations. Our analysis of local bifurcations used the computer programs Macsyma, Mathematica and Maple. For  $y = m, n$  or  $h$  the equation for  $\dot{y}$  in HH is linear in  $y$ , so the last three components of an equilibrium solution  $(V_*, M_*, N_*, H_*)$  of HH can be written as functions of  $V_*$ :

$$y_* = y_\infty(V_*) = \frac{\alpha_y(V_*)}{\alpha_y(V_*) + \beta_y(V_*)} \quad \text{for } y = m, n, h.$$

Substituting  $y_*$  for  $y = m, n, h$  in the first equation we obtain:

$$G(V_*, m_\infty(V_*), n_\infty(V_*), h_\infty(V_*)) = f(V_*) = I. \tag{1}$$

Thus, for fixed  $\bar{V}_K$  there is exactly one value of  $I$  for which  $(V_*, m_*, n_*, h_*)$  is at equilibrium. Note that derivatives of HH are independent of  $I$ .

When  $\bar{V}_K$  has the HH value of +12 mV,  $f$  is monotonic and HH has a unique equilibrium for each value of  $I$ . For fixed lower values of  $\bar{V}_K$  there are two saddle

node bifurcations as  $I$  is varied, creating a region with three equilibria. The two curves of saddle nodes terminate at a cusp point; see also Holden *et al.* (1985). The saddle node curves in the  $I \times \bar{V}_K$  plane were computed parametrically with  $V_*$  as the independent parameter. The equations describing the saddle node curves involve the determinant of the matrix of first derivatives of HH at an equilibrium point. We calculated an explicit expression for this determinant symbolically with the computer programs Macsyma, Maple and Mathematica. By solving the equation which the determinant vanishes for  $\bar{V}_K$  at equilibrium values of  $(V_*, m_*, n_*, h_*)$ , we obtained the curve  $\bar{V}_K(V_*)$  of parameter values corresponding to zero eigenvalues.

To determine the parameter values at which Hopf bifurcation occurs, it is necessary to compute eigenvalues of the matrix of first derivatives of HH at an equilibrium point. There is a pair of purely imaginary eigenvalues when the characteristic polynomial  $x^4 + c_3x^3 + c_2x^2 + c_1x + c_0$  of this matrix satisfies simultaneously the third degree equation  $c_1^2 + c_0c_3^2 - c_1c_2c_3 = 0$  and the inequality  $c_1c_3 > 0$ . Again, we computed this equation symbolically, assuming a given value of  $V_*$ , and solved it for  $\bar{V}_K$ . The graph we obtained for the solution of this equation and inequality disagrees slightly with the findings of Holden *et al.* (1983) for the HH value of  $\bar{g}_K$ . Takens–Bogdanov bifurcations occur when the equations defining Hopf bifurcations and saddle node bifurcations are satisfied simultaneously.

The saddle node and Hopf bifurcations are the only codimension one bifurcations that can be computed explicitly from HH without numerical integration. The presence of double cycles where the two periodic orbits created at Hopf bifurcation points coalesce and disappear has been established previously (Hassard and Shiau, 1987; Labouriau, 1989; Rinzel and Miller, 1980) and the existence of saddle loops emanating from the (tb) points is predicted by bifurcation theory (Guckenheimer and Holmes, 1983). To determine further information about global bifurcation we rely upon numerical integrations that were performed with the computer programs *kaos* and *DsTool* (Back *et al.*, 1992). These programs establish a graphical interface and display for investigating bifurcations of dynamical systems. They allow one to mark points in a two-dimensional parameter space with identifying symbols and to display phase portraits that correspond to these points. The computed data for local bifurcations were displayed in the parameter space window. By searching for the boundaries of parameter regions yielding structurally stable dynamics and using our knowledge of the unfoldings of codimension two bifurcations, we deduced the location of curves along which global bifurcations occur. We obtain a consistent picture of the bifurcation diagrams for HH in the two-dimensional  $I \times \bar{V}_K$  parameter plane. These diagrams have not been proved to be correct, but they are based upon strong numerical evidence.

A qualitative depiction of the bifurcation diagram resulting from our

numerical investigations is shown in Fig. 1. It is difficult to adequately depict the different regimes on an accurate diagram since some of the regions are very small. Figure 2 shows two phase portraits for  $(vk, I) = (-7, -0.03647)$  and  $(vk, I) = (-5.155, -0.03647)$ . Figure 2a shows a phase portrait with a single equilibrium point (a saddle with two stable and two unstable eigenvalues depicted by a cross) and a stable limit cycle projected onto the  $(h, v)$  plane. In Fig. 2b there are three equilibrium points. The saddles are depicted by crosses and the sink is depicted by a triangle. The middle saddle in this picture has a single unstable eigenvalue, and of the separatrices of the unstable manifold of this point is involved in the global bifurcations that are illustrated in Figs 3 and 4.

Prominent features of the bifurcation diagram in Fig. 1 include a curve of double cycles (dc), which enters the cusp region with three equilibrium points and terminates at a degenerate Hopf bifurcation (dh) close to the Takens–Bogdanov point (tb). These double cycles are the ones described by Labouriau (1989). The curve of saddle loops (sl) emanating from the Takens–Bogdanov point crosses the Hopf curve beyond the degenerate Hopf point and then turns sharply. From this sharp bend, it proceeds almost parallel to the saddle node curve (sn). Details of the phase portraits in this part of the bifurcation diagram are shown in Fig. 3. A section is drawn across the diagram with  $I = -0.03647$  and values of  $vk$  ( $-5.155, -5.153, -5.15, -5.14822, -5.1482$  and  $-5.129$ ) that lie in six different regions of the bifurcation are used to compute phase portraits. In the first five of these regions there are three equilibrium points, two of which are shown in Figs 3a–e. One of these equilibrium points is a saddle with one unstable eigenvalue throughout the region. We illustrate the differences in the dynamical behavior by drawing part of one unstable separatrix for this saddle, projected into the  $(h, v)$  plane. The diagrams show the saddle point as a cross in the upper right portion of each diagram. A second equilibrium point appears in the diagrams. In Figs 3a and b the parameters lie to the left of the bifurcation curve and the second equilibrium is a saddle with a pair of complex, unstable eigenvalues. In Figs 3c, d and e the second equilibrium is a sink. In Fig. 3a the unstable separatrix approaches a stable limit cycle (only part of which is shown so that the behavior near the saddle can be seen more clearly). Between Figs 3a and b a saddle loop bifurcation occurs so that the separatrix in Fig. 3b tends to the third equilibrium point, a sink that is not shown. The Hopf bifurcation occurs between Figs 3b and c. Between Figs 3c and d the saddle loop branch of bifurcations is crossed once more and in Fig. 3d the stable limit cycle coexists with two sinks in the flow. Between Figs 3d and e, the branch of double cycles is crossed. The separatrix in Fig. 3e tends to the sink in the diagram. Finally, Fig. 3f shows part of the trajectory in the parameter region where there is a single equilibrium point, the sink that lies outside the diagram.

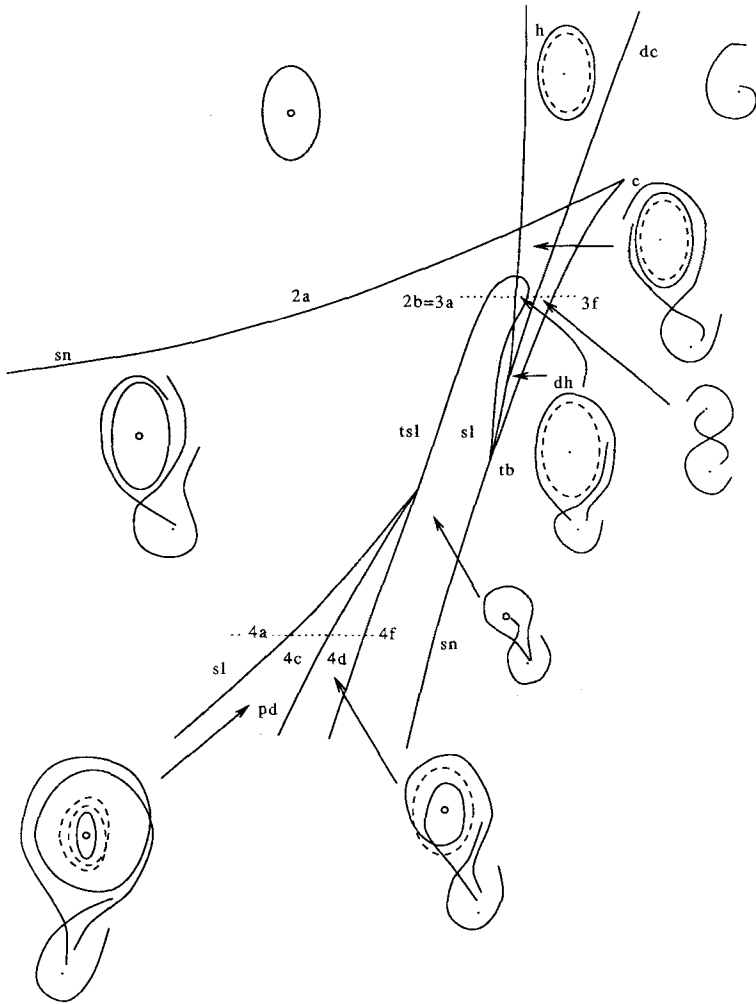


Figure 1. Schematic representation of the bifurcation diagram for HH on the  $I \times \bar{V}_K$  plane with  $\bar{g}_K = 36$ . Phase portraits for each region in the two-dimensional diagram are shown. Stable equilibrium points are shown as solid dots, saddle points with two-dimensional unstable manifolds are unfilled dots, stable limit cycles are closed curves with solid lines and unstable periodic orbits are dashed lines. One dimensional unstable manifolds of equilibrium points are shown together with curves of the “weak stable manifolds” of equilibrium points with three-dimensional stable manifolds. The bifurcation curves and codimension two bifurcations are labeled with abbreviations described in the text. The numbers and dotted lines correspond to the location of parameter values, for which numerically computed phase space information is displayed in Figs 2, 3 and 4.

As the curve of saddle loop bifurcations is followed beyond the region described above, two events occur. First, the twist type of the saddle loop changes at a point we have not identified. Second, a point of codimension two bifurcation at which there is twisted neutral saddle loop occurs close to  $(vk, I) = (-6.1, -0.7)$ . As described by Chow *et al.* (1988) there are three codimension one curves passing through this codimension two point in the bifurcation diagram. Figure 4 shows phase portraits for six different values of  $vk$  ( $-7.158, -7.157549, -7.15753, -7.15744, -7.1574388, -7.157$ ) with  $I = -1.65$ . Throughout this region there are three equilibrium points, but only the saddle with a single unstable real eigenvalue is shown. Figure 4a with  $vk = -7.158$  shows one of the unstable separatrices of this saddle accumulating on a stable limit cycle in an oscillatory manner. Figure 4b represents a parameter value very close to the untwisted saddle loop. Figure 4c has parameters that lie between the saddle loop and period doubling bifurcations. The unstable separatrix tends to a sink that lies above the picture, but there is still a stable limit cycle. This limit cycle becomes unstable as the period doubling bifurcation curve is crossed. Figure 4d shows the separatrix together with a portion of another trajectory that begins near the unstable equilibrium point outside the picture and proceeds past the saddle to the sink. Figure 4e comes from a parameter value that is close to the twisted, "once-rounding" saddle loop. Figure 4f shows the separatrix at parameter values farther to the right of the twisted saddle loop.

When  $\bar{g}_K$  is decreased from the HH value of  $36 \text{ mS/cm}^{-2}$  the Takens-Bogdanov point in the  $I \times \bar{V}_K$  plane moves towards the cusp point and past it.

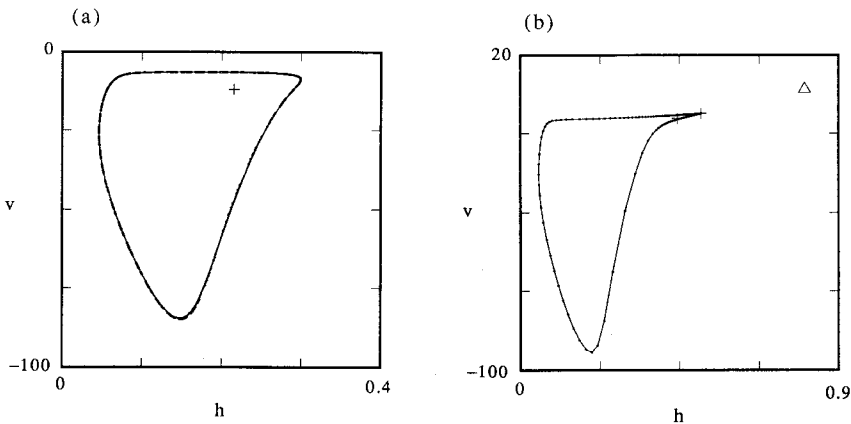


Figure 2. Two phase portraits for parameter values (a)  $(vk, I) = (-7, -0.03647)$  and (b)  $(vk, I) = (-5.155, -0.03647)$  from the bifurcation diagram depicted in Fig. 1. The phase space is projected onto the  $(h, v)$  coordinate plane. Stable equilibrium points are marked by triangles and saddle points are marked by crosses. Stable limit cycles are plotted.

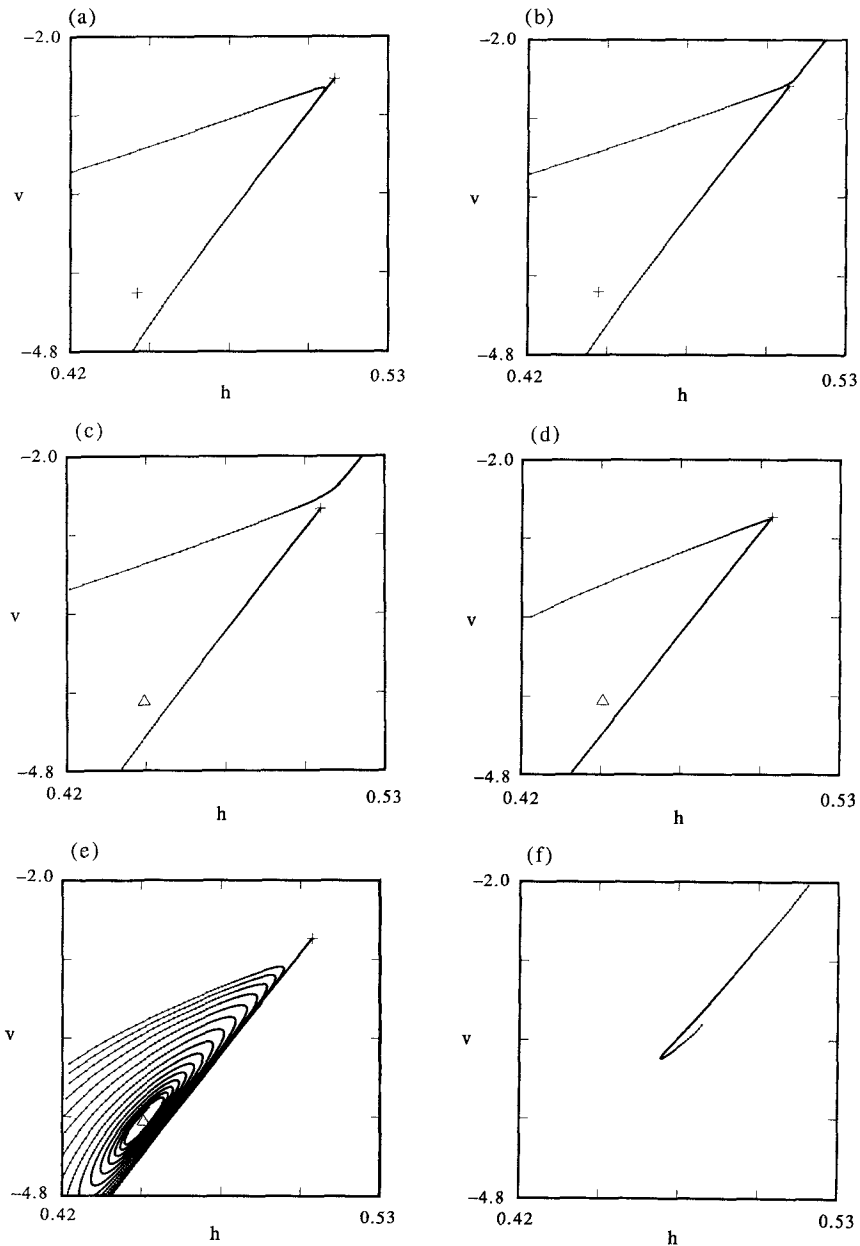


Figure 3. Details of six-phase portraits corresponding to different parameter values in Fig. 1. The phase space is projected onto the  $(h, v)$  coordinate plane. In all cases  $I = -0.03647$ . The values of  $vk$  are: (a)  $-5.155$ , (b)  $-5.153$ , (c)  $-5.15$ , (d)  $-5.14822$ , (e)  $-5.1428$  and (f)  $-5.129$ . In phase portraits (a)–(e) a single unstable separatrix of a saddle indicated by a cross is shown. A second equilibrium point is denoted by a cross (saddle) or triangle (sink). The trajectories that leave the bottom of the region return through the left-hand side. In all cases there is a stable equilibrium point above and to the right of the region of phase space in the diagram.

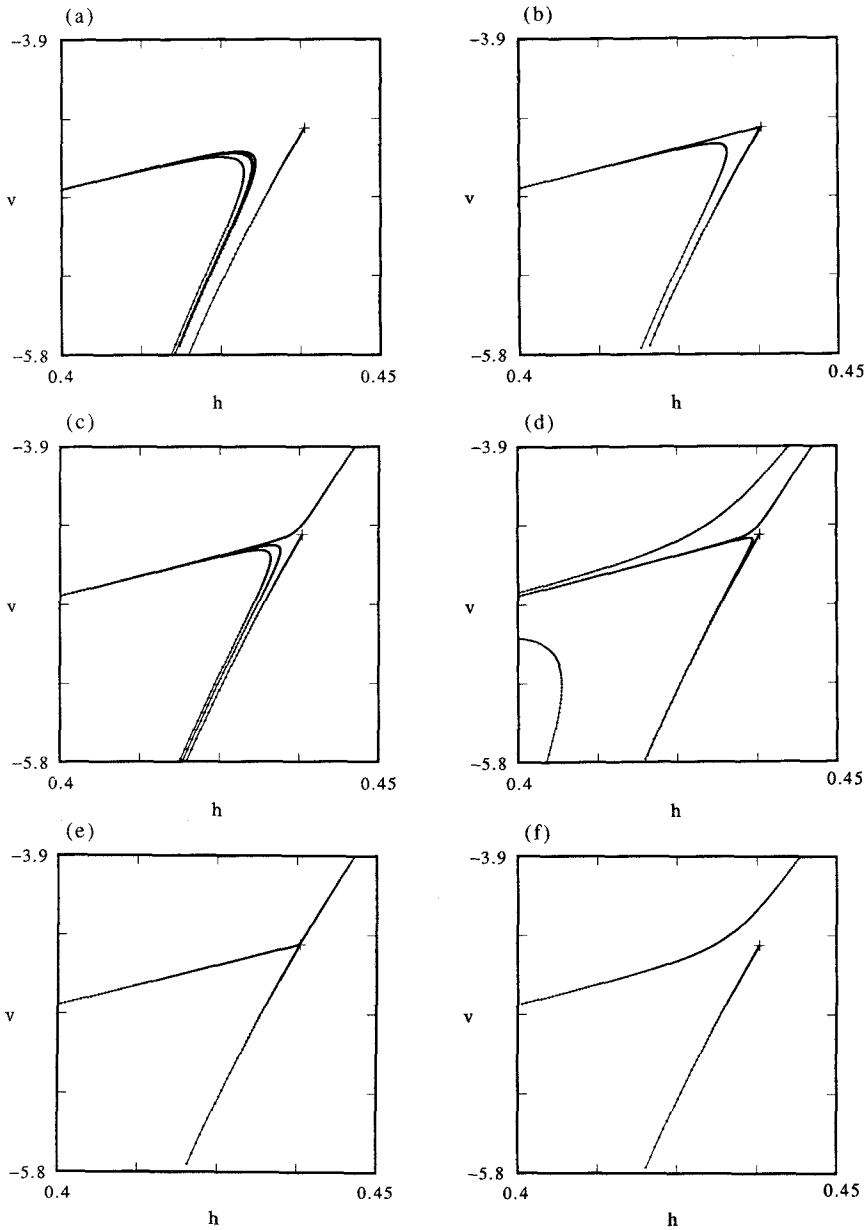


Figure 4. Details of six phase portraits corresponding to different parameter values in Fig. 1. The phase space is projected onto the  $(h, v)$  coordinate plane. In all cases  $I = -1.65$ . The values of  $vk$  are: (a)  $-7.158$ , (b)  $-7.157549$ , (c)  $-7.15753$ , (d)  $-7.15744$ , (e)  $-7.1574388$  and (f)  $-7.157$ . In (a), (b), (e) and (f) a single unstable separatrix of a saddle point is plotted. In (c) a portion of a stable limit cycle (between the two “passes” of the separatrix) is shown, in addition to the unstable separatrix. In (d) a portion of a trajectory that starts near an equilibrium to the left of the figure is shown. Trajectory segments that exit from the bottom of the plots return through the left-hand side.

This agrees qualitatively with the findings of Holden *et al.* (1985), but their results differ from ours in the value of  $\bar{g}_K$ , for which the Takens–Bogdanov point moves past the cusp. The unfolding for the codimension three bifurcation in which cusp and Takens–Bogdanov bifurcations coincide has been analysed by Guckenheimer (1986) and Dumortier *et al.* (1987). The geometry of the unfolding of this codimension three bifurcation can be visualized by drawing a two-dimensional sphere that encloses the codimension three point in the three-dimensional parameter space of the unfolding (Guckenheimer, 1986).

To further explore the effect of this codimension three bifurcation on the bifurcation diagrams of HH we decreased  $\bar{g}_K$  from the HH value of 36 mS/cm<sup>2</sup> to 12 mS/cm<sup>2</sup> and computed another bifurcation diagram in the  $I \times \bar{V}_K$  plane. The new bifurcation diagram is shown in Fig. 5. Among its features are a curve of double cycles (dc) that terminates at a neutral saddle loop point (nsl) near  $(vk, I) = (-0.6824, 1.9088)$  instead of a double Hopf bifurcation as in the unfolding of the codimension three bifurcation. The point (nsl) does not lie on the saddle loop branch emanating from the Takens–Bogdanov point (tb), however. Instead it ends on a saddle loop that encloses both equilibrium points. This branch of saddle loops ends on both branches of saddle nodes at saddle node loops (snl). The codimension two point is located very close to the upper branch of saddle nodes.

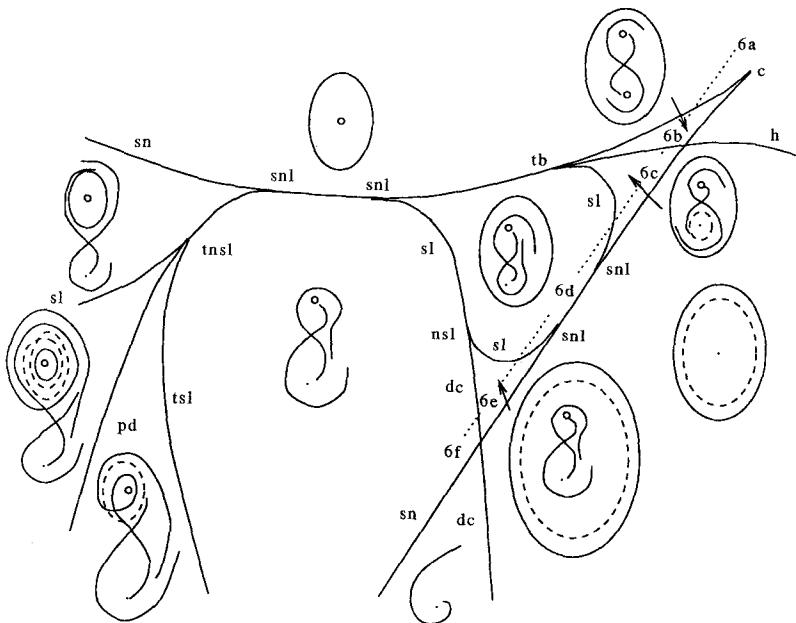


Figure 5. Schematic bifurcation diagram and phase portraits on the two-dimensional invariant manifold for HH with  $\bar{g}_K = 12$  on the  $I \times \bar{V}_K$  plane. The conventions are the same as those of Fig. 1.

Some of the details of the portion of the bifurcation diagram near the cusp are illustrated in the phase portraits shown in Fig. 6. Parameter values are selected along a line  $6vk - 5I = 27.3$  in the  $(vk, I)$  plane that is approximately parallel to the saddle node curve that forms one side of the cusp. Figure 6a corresponds to  $(vk, I) = (8.6, 4.86)$  and gives a phase portrait outside the cusp region. There is a single equilibrium point and a stable limit cycle. Figure 6b is inside the cusp region of the bifurcation diagram within  $(vk, I) = (7.3, 3.3)$ . There are no sinks and the limit cycle attracts almost all trajectories. Figure 6c with  $(vk, I) = (7.2, 3.18)$  lies on the opposite side of the Hopf curve and has a sink, but the saddle separatrices of the middle saddle still tend to the limit cycle. Between Figs 6c and d, there is a saddle loop bifurcation at which the unstable periodic orbit created in the Hopf bifurcation disappears. In Fig. 6d, with  $(vk, I) = (7.125, 3.09)$ , there is still a stable limit cycle, but one unstable separatrix now tends to the stable equilibrium. Between Figs 6d and e there is a second saddle loop bifurcation and a new unstable periodic orbit is created that "surrounds" all three equilibrium points. In Fig. 6e, with  $(vk, I) = (7.1, 3.06)$ , both saddle separatrices tend to the stable equilibrium. Finally, stable and unstable periodic orbits collide in a double cycle bifurcation between Figs 6e and f. In Fig. 6f with  $(vk, I) = (7.05, 3)$ , no periodic orbits remain and almost all trajectories tend to the stable equilibrium.

The branch of twisted saddle loops (tsl) that was present at the higher value of  $\bar{g}_K$  remains. It starts on the saddle node curve at another saddle node loop. The twisted saddle loops still pass through a neutral point (tnsl) near  $(vk, I) = (-4.16922, 1.400666)$ , at which bifurcation curves of period doublings (pd) and doubled saddle loops (dsl) originate. Our proposed bifurcation diagrams for HH near the cusp points appear to be compatible with the unfolding of the Takens-Bogdanov cusp codimension three bifurcation, although the diagrams drawn here are sufficiently far from the codimension three bifurcation that significant differences with its unfolding exist.

**5. Discussion.** Our results illustrate the complexity of patterns of multiple attracting states and bifurcation in the HH equations. There are many possibilities for the patterns of repetitive response and single action potentials as the coefficients of HH vary. Much of the complexity that we find is confined to small regions of the parameter space, however. Finding some of the patterns experimentally may be difficult for this reason. Even so, our bifurcation diagrams can be used to make predictions about periodicity and hysteresis in space clamped experiments on squid axons. Slowly varying the imposed potential  $I$  in such an experiment corresponds to moving along a line of constant  $\bar{V}_K$  in the  $I \times \bar{V}_K$  plane. By varying both ionic concentration of potassium and the voltage potential in an experiment, it may be possible to produce experimental versions of the bifurcation diagrams presented here.

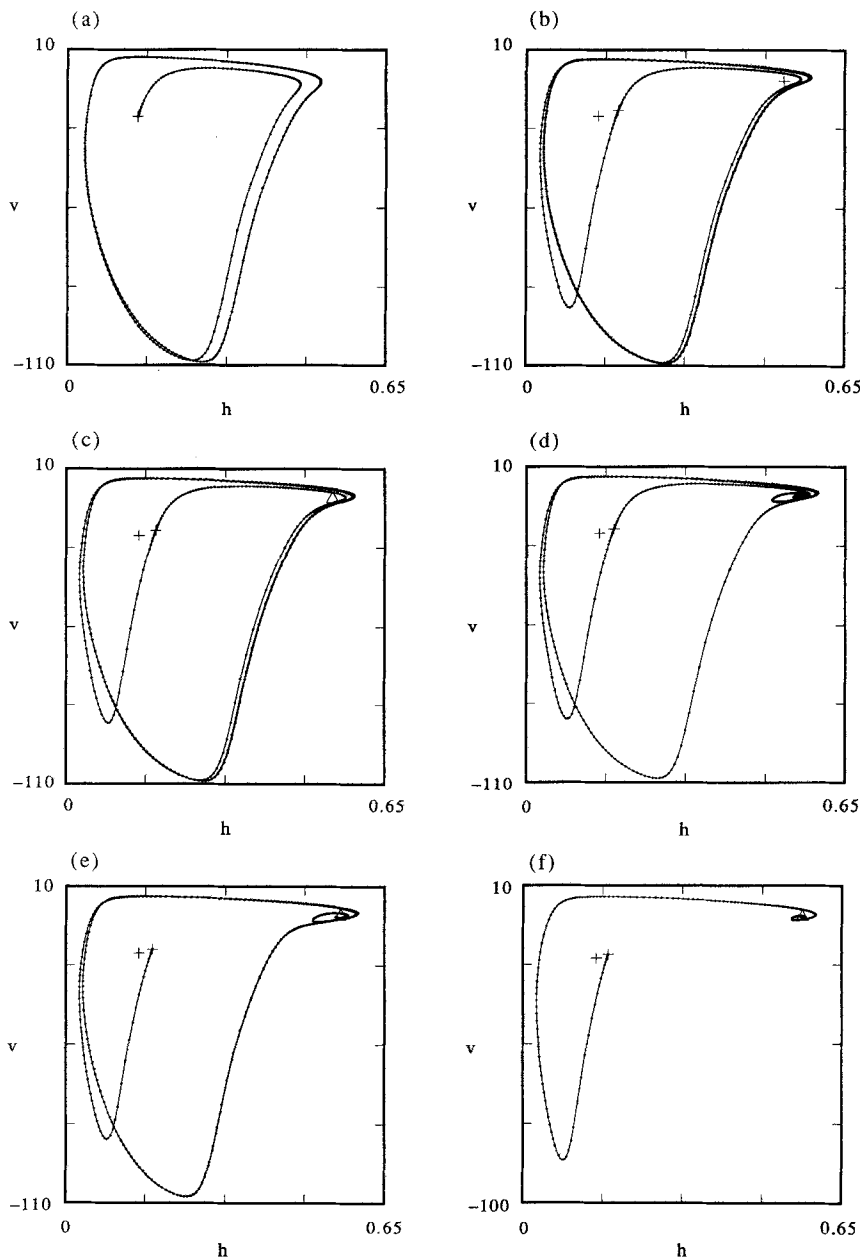


Figure 6. Phase portraits for six different parameter values shown in Fig. 5: (a) (8.6, 4.86), (b) (7.3, 3.3), (c) (7.2, 3.18), (d) (7.125, 3.09), (e) (7.1, 3.06) and (f) (7.05, 3). The phase space is projected onto the  $(h, v)$  coordinate plane. In (a), (e) and (f) one unstable separatrix of the middle saddle point is shown. In (b), (c), and (d) both unstable separatrices of the middle saddle are shown. In (e) a stable limit cycle that is not the limit of the unstable separatrix is plotted.

Matching experimental data to the bifurcation diagrams of models may provide a sensitive test for discriminating among models and estimating model parameters. Such studies have been undertaken for homogeneous chemical reactors (Maselko *et al.*, 1986), but the inability to efficiently compute the bifurcation diagrams for realistic models has been a limiting factor in the use of this type of analysis. Our work introduces computational tools that overcome this difficulty for the Hodgkin–Huxley model of voltage-clamped action potentials in squid axons. The use of these methods to make comparisons between experimental data and compartmental models of a conditionally bursting neuron have been pursued by Guckenheimer *et al.* (1993).

Simpler models of action potential for nerve impulses based upon planar vector fields have been extensively studied. While these models display many aspects of solutions to the Hodgkin–Huxley equations (Fitzhugh, 1961; Kepler *et al.*, 1992; Nagumo *et al.*, 1900), some of the features of HH dynamics described here cannot be found in systems of planar vector fields. In particular, the twisted homoclinic orbits that we find in the Hodgkin–Huxley system cannot occur in planar systems for topological reasons. Thus, our analysis provides a means of demonstrating the inherent limitations in aggregating variables in the HH system to produce a planar vector field with the same qualitative properties as the original equations.

## LITERATURE

- Back, A., J. Guckenheimer, M. Myers, F. Wicklin and P. Worfolk. 1992. dstool: Computer Assisted Exploration of Dynamical Systems, Notices of the American Mathematical Society, Vol. 39, pp. 303–309.
- Bogdanov, R. I. Trudi Sem. Petrovsk. 2. 1976. English translation: Versal deformation of a singularity of a vector field on the plane in the case of zero eigenvalue, *Sel. math. Sov.* **1**, 389–421.
- Chow, S. N., B. Deng and B. Fiedler. 1988. *Homoclinic Bifurcation at Resonant Eigenvalues*. Knorad-Zuse-Zentrum für Informationstechnik, F.R.G. Preprint SC-88-10.
- Dangelmayr, G. and J. Guckenheimer. 1987. On a four parameter family of planar vector fields, *Arch. Rat. Mech. Anal.*, 321–352.
- Dumortier, F., R. Roussarie and J. Sotomayor. 1987. *Generic 3-parameter families of vector fields on the plane, unfolding a singularity with nilpotent linear part. The cusp case of codimension 3*. In: *Ergodic Theory and Dynamical Systems*, Vol. 7, pp. 375–413.
- Fitzhugh, R. 1961. Impulses and physiological states in models of nerve membranes, *Biophys. J.* **1**, 445–466.
- Golubitsky, M. and D. G. Schaeffer. 1985. *Singularities and Groups in Bifurcation Theory*, Vol. I. Berlin: Springer-Verlag.
- Guckenheimer, J. 1986. Multiple bifurcation problems for chemical reactions, *Physica* **20D**, 1–20.
- Guckenheimer, J. and P. Holmes. 1983. *Nonlinear Oscillations, Dynamical Systems and Bifurcations of Vector Fields*. Berlin: Springer-Verlag.
- Guckenheimer, J. and S. Kim. 1990. *kaos* Mathematical Sciences Institute Technical Report. Cornell University, Ithaca NY.

- Guckenheimer, J., S. Gueron and R. M. Harris-Warrick. 1993. Mapping the dynamics of a bursting neuron, *Phil. Trans. Roy. Soc. Lond.* (in press).
- Guttman, R., S. Lewis and J. Rinzel. 1980. Control of repetitive firing in squid giant axon as a model for a neurone oscillator, *J. Physiol.* **305**, 377–395.
- Hassard, B. D. and L. J. Shiau. 1987. Isolated periodic solutions of the Hodgkin–Huxley model nerve conduction equations. Preprint. Department of Mathematics, SUNY at Buffalo.
- Hille, B. 1992. *Ionic Channels of Excitable Membranes*, Sinauer.
- Hodgkin, A. L. and A. F. Huxley. 1952(a). Current carried by sodium and potassium ions through the membrane of the giant axon of Loligo. *J. Physiol.* **116**, 449–4723.
- Hodgkin, A. L. and A. F. Huxley. 1952(b). A quantitative description of membrane current and its applications to conduction and excitation in nerve. *J. Physiol.* **117**, 500–544.
- Holden, A. V., M. A. Muhamad and A. K. Schierwagen. 1985. Repolarizing currents and periodic activity in nerve membrane. *J. theoret. Neurobiol.* **4**, 61–71.
- Jack, J. J. B., D. Noble and R. W. Tsien. 1975. *Electric Current Flow in Excitable Cells*. Oxford: Clarendon Press.
- Kepler, T. B., L. F. Abbott and E. Marder. 1992. Reduction of conductance-based neuron models. Preprint. Brandeis University.
- Kokubu, H. 1988. Homoclinic and heteroclinic bifurcations of vector fields. *Japan J. appl. Math.* **5**, 455–501.
- Labouriau, I. S. 1989. Degenerate Hopf bifurcation and nerve impulse, Part II. *SIAM J. math. Anal.* **20**, 1–12.
- Maselko, J., M. Alagami and I. Epstein. 1986. Bifurcation analysis of a system of coupled chemical oscillators: bromate-chlorite-iodide. *Physica* **19D**, 153–161.
- Nagumo, J. S., S. Arimoto and R. Seitz. An active pulse transmission line simulating nerve axon. *Proc. IRE*, 2061–2070.
- Rinzel, J. and R. N. Miller. 1980. Numerical solutions of the Hodgkin–Huxley equations. *Math. Biosci.* **49**, 27–59.
- Schechter, S. 1987. The saddle node separatrix loop. *SIAM J. math. Anal.* **18**, 1142–1156.
- Takens, F. 1974. Forced oscillations and bifurcations, applications of global analysis, Vol. 3, 1–59. Rijksuniversiteit, Utrecht: Communications of Maths Institute.
- Thom, R. 1975. *Structural Stability and Morphogenesis*. Reading, MA: Benjamin.
- Yanagida, E. 1987. Branching of double pulse solutions from single pulse solutions in nerve axon equations. *J. diff. Eq.* **66**, 243–262.

Received 4 May 1992

Revised 23 November 1992